

# Principal component proxy tracer analysis

**Peter Mills**

*peteymills@hotmail.com*

November 26, 2021

## **Abstract**

We introduce a powerful method for dynamical reconstruction of long-lived tracers such as ozone. It works by correlating the principal components of a matrix representation of the tracer dynamics with a series of sparse measurements. The method is tested on the 500 K isentropic surface using a simulated tracer and with ozone measurements from the Polar Aerosol and Ozone Measurement (POAM) III satellite instrument. The Lyapunov spectrum is measured and used to quantify the lifetime of each principal component. Using a 60 day lead time and five (5) principal components, cross validation of the reconstructed ozone and comparison with ozone sondes return root-mean-square errors of 0.20 ppmv and 0.47 ppmv, respectively.

## **Keywords**

**tracer dynamics, interpolation, inverse methods, remote sensing, chaos in the atmosphere, data assimilation, ozone**

## **1 Introduction**

Randall et al. (2002) demonstrate a method for proxy tracer reconstruction of ozone that works by correlating sparse measurements from satellites or other remote-sensing instruments with conserved tracer fields such as potential vorticity. The proxy tracer method is an approximate interpolation

method, appropriate for long-lived tracers such as ozone, that takes into account the wind dynamics. Here we demonstrate a similar method in which the tracer dynamics are represented as a matrix. The matrix is decomposed using principal component analysis (PCA), also called singular value decomposition (SVD), and the largest principal components then fitted to the measurements.

## 2 Background

Consider a system of ordinary differential equations:

$$\frac{d\mathbf{x}}{dt} = \mathbf{f}(\mathbf{x}, t) \quad (1)$$

We linearize this about  $\mathbf{x}$ :

$$\frac{d}{dt}(\mathbf{x} + \delta\mathbf{x}) \approx \mathbf{f} + \nabla\mathbf{f} \cdot \delta\mathbf{x} \quad (2)$$

$$\frac{d}{dt}\delta\mathbf{x} \approx \nabla\mathbf{f} \cdot \mathbf{x} \quad (3)$$

Define  $H$  such that:

$$\frac{d}{dt}H = \nabla\mathbf{f} \cdot H \quad (4)$$

$$H(t=0) = I \quad (5)$$

where  $I$  is the identity matrix. This is what is known as the *tangent model* which we decompose using principal component analysis (PCA), also called singular value decomposition (SVD) or empirical orthogonal function (EOF) analysis:

$$H = U \cdot S \cdot V^T \quad (6)$$

where  $U$  and  $V$  are orthonormal matrices while  $S$  is diagonal and contains the *singular values* (Press et al., 1992). The matrix  $U$  contains the *left singular vectors* while  $V$  contains the *right singular vectors*. The terms principal component (PC) and singular vector will be used interchangeably to denote a left singular vector.

Singular vectors are increasingly being used in meteorology to quantify the predictability of a forecast or to generate perturbations for ensemble

forecasts (Tang et al., 2006). An Eulerian tracer simulation is linear, that is the tangent vector is simply the dynamics. Thus:

$$\mathbf{x}_j \approx H_j \cdot \mathbf{x}_0 \quad (7)$$

where  $\mathbf{x}_j = \mathbf{x}(t_j)$  is a gridded representation of a passive flow tracer at the  $j$ th time step.  $H_j = A_j \cdot A_{j-1} \cdot A_{j-2} \cdot \dots \cdot A_3 \cdot A_2 \cdot A_1$  is the tracer dynamics and the matrix  $A_j$  maps  $x_{j-1}$  to  $x_j$ . We can say that:

$$A_j = \int_{t_{j-1}}^{t_j} \nabla \mathbf{f} dt \quad (8)$$

The Lyapunov exponents are defined as the logarithms of the time averages of the singular values in the limit as time goes to infinity:

$$\lambda_i = \lim_{t \rightarrow \infty} \frac{1}{t} \log s_i; \quad \lambda_{i-1} \leq \lambda_i \quad (9)$$

where  $s_i$  is the  $i$ th singular value (Ott, 1993). For most systems:

$$|\delta \mathbf{x}| \approx |\delta \mathbf{x}(0)| \exp(\lambda_i) \quad (10)$$

That is, as  $H$  is integrated forward, the largest singular value and the largest singular vector will increasingly begin to dominate (Ott, 1993).

### 3 Numerics and data

To run the tracer advection, the *ctraj* software package is used (<http://ctraj.sf.net>). The codes are written in C++ and contain programs for gridded, semi-Lagrangian tracer advection on an azimuthally-equidistant-projected coordinate system. Two fields are advected simultaneously, one for the Northern hemisphere and one for the Southern hemisphere, with equatorial crossings accounted for. Gridding on both hemispheres is 100 by 100, or 200km-, 1.8 degree-latitude-separation at the pole. Output is written to a series of sparse matrices which are then decomposed with the Lanczos method (Golub and van Loan, 1996) using the Arnoldi package (ARPACK) (Lehoucq and Scott, 1996).

The Polar Ozone and Aerosol Measurement (POAM) III instrument is a solar-occultation instrument mounted on a sun-synchronous, low-earth-orbit satellite (Lucke et al., 1999). Using optimal estimation (Rodgers, 2000),

ozone profiles are retrieved within a narrow latitude band in either polar region (Lumpe et al., 2002). It is capable of returning 28 or 29 measurements per day, alternating between Northern and Southern hemisphere, however because of a malfunction in the instrument, it normally operates in only one or the other hemisphere for longer periods. Therefore, we confine ourselves to earlier data, October and November 1998, when more frequent and diverse measurements are available.

The National Center for Environmental Prediction (NCEP) supplies, free-of-charge, gridded (2.5 by 2.5 degrees longitude/latitude, 4 time daily), re-analyzed climate data starting in 1948 (Kalnay et al., 1996). Wind and temperature data is used to drive the advection model.

## 4 Tracer correlation

Two differently-initialized tracers, when integrated with the same wind fields over a long time period, become correlated. This can be used to infer global fields of a long-lived tracer such as ozone based on only a few sparse measurements (Allen and Nakamura, 2003; Randall et al., 2002). Figure 1 demonstrates this with the extreme example of an initially zonally-symmetric tracer and an initially meridionally-symmetric tracer. Tracers are advected with National Center for Environmental Prediction (NCEP) reanalysis 1 data at the 500 K isentrop (Kalnay et al., 1996).

We also plot the correlation of the first tracer with the largest singular vector. We see that, because of Equation (10), they too become correlated over time. This at least partially explains the efficacy of the proxy tracer method. A sample PC as compared with the tracer is shown in Figure 2.

Figure 3 plots the time evolution of the singular values. From this we can calculate the Lyapunov spectrum by making straight line fits of their logarithms. While the resulting fields may develop into complex fractals (Mills, 2009) the Lyapunov spectrum shows that the tracer dynamics themselves are not truly chaotic, but are only on the cusp: the largest singular value remains approximately constant. It also shows how quickly the other singular vectors decay, so that the largest will eventually dominate in accordance with Equation 10.

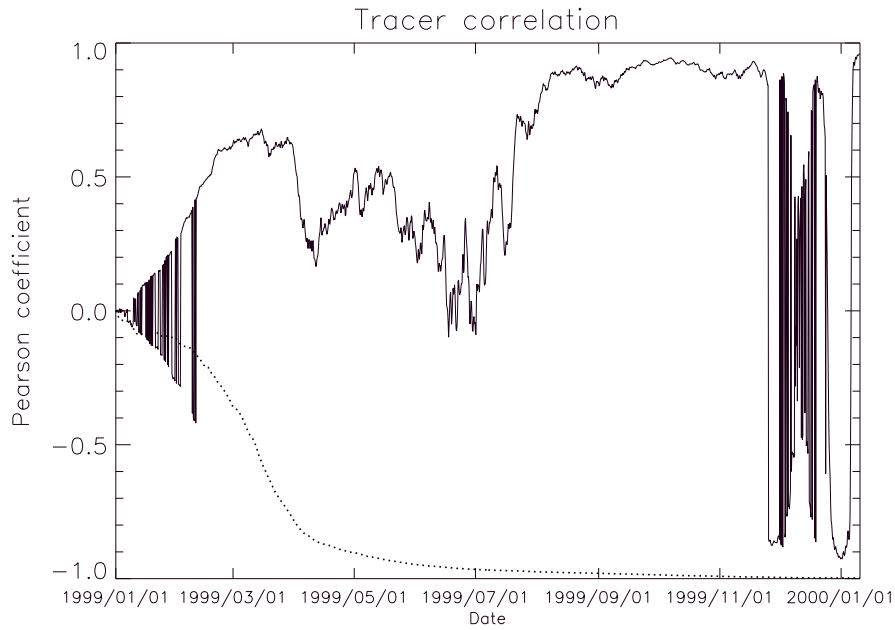


Figure 1: The correlation over time of two differently-initialized tracers (broken line)—zonally symmetric and meridionally symmetric—and of the zonally-symmetric-initialized tracer with the first principal component. The simulation was driven with NCEP reanalysis 1 data on the 500 K isentropic level with an Eulerian time-step of six (6) hours and a Lagrangian time-step of one (1) hour.

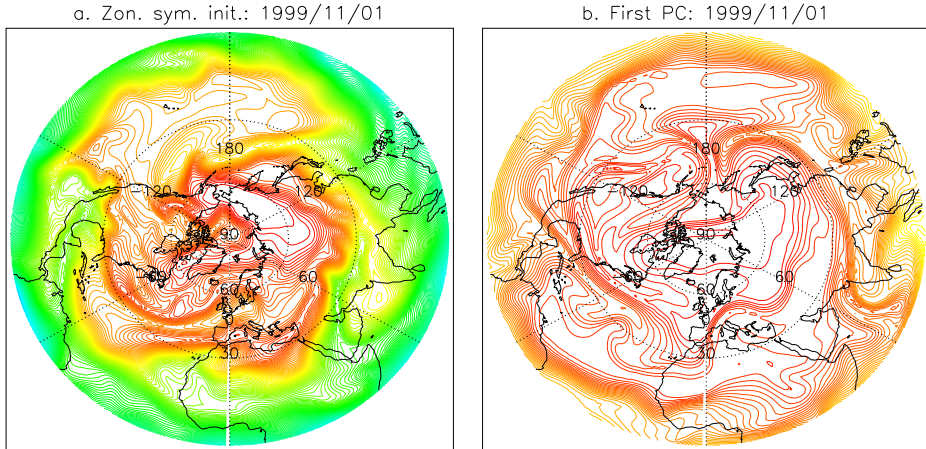


Figure 2: Comparison of a simulated tracer (a.) and the first principal component (b.) for the same time integration.

## 5 Principal component proxy

Principal component proxy analysis works by linearly regressing the largest singular vectors with the measurements. Since the measurements will likely not occur all at the same time, we must first generate the right singular vectors for a given tracer mapping,  $H_j$ , at *lead time*  $j$ , then generate a series of left singular vectors for different time steps by applying the tracer mapping. For the right singular vectors, ARPACK is used to compute the eigenvectors of  $H_j^T \cdot H_j$ . Values interpolated within the right singular vectors at the measurement locations are fitted through coefficients,  $\{c_i\}$ , to the measurements. Thus, we need to fit the following equation:

$$\sum_{i=1}^m c_i \mathbf{w}_k \cdot H_k \cdot \mathbf{v}_i = q_k \quad (11)$$

where  $m$  is the number of singular vectors used in the analysis,  $q_k$  is the measurement at time step  $k$  (we assume that each measurement has a unique time stamp),  $H_k$  is the tracer mapping at time  $k$ ,  $w_k$  is a vector of interpolation coefficients and  $\mathbf{v}_i$  is the  $i$ th right principal component. The fitting is done using a linear least squares (Galassi et al., 2007).

To perform the analysis, we need to choose a lead time, as well as a *measurement window*. The lead time determines how long the tracer is ad-

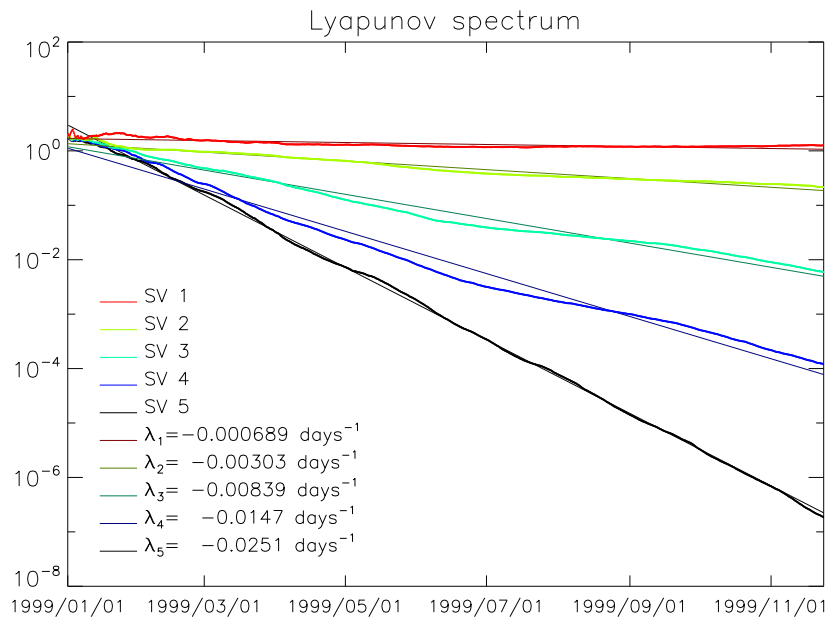


Figure 3: Plot of the top five (5) singular-values of a semi-Lagrangian tracer simulation over time. Straight-line fits return the Lyapunov-spectrum. The simulation was done on the 500 K isentropic level.

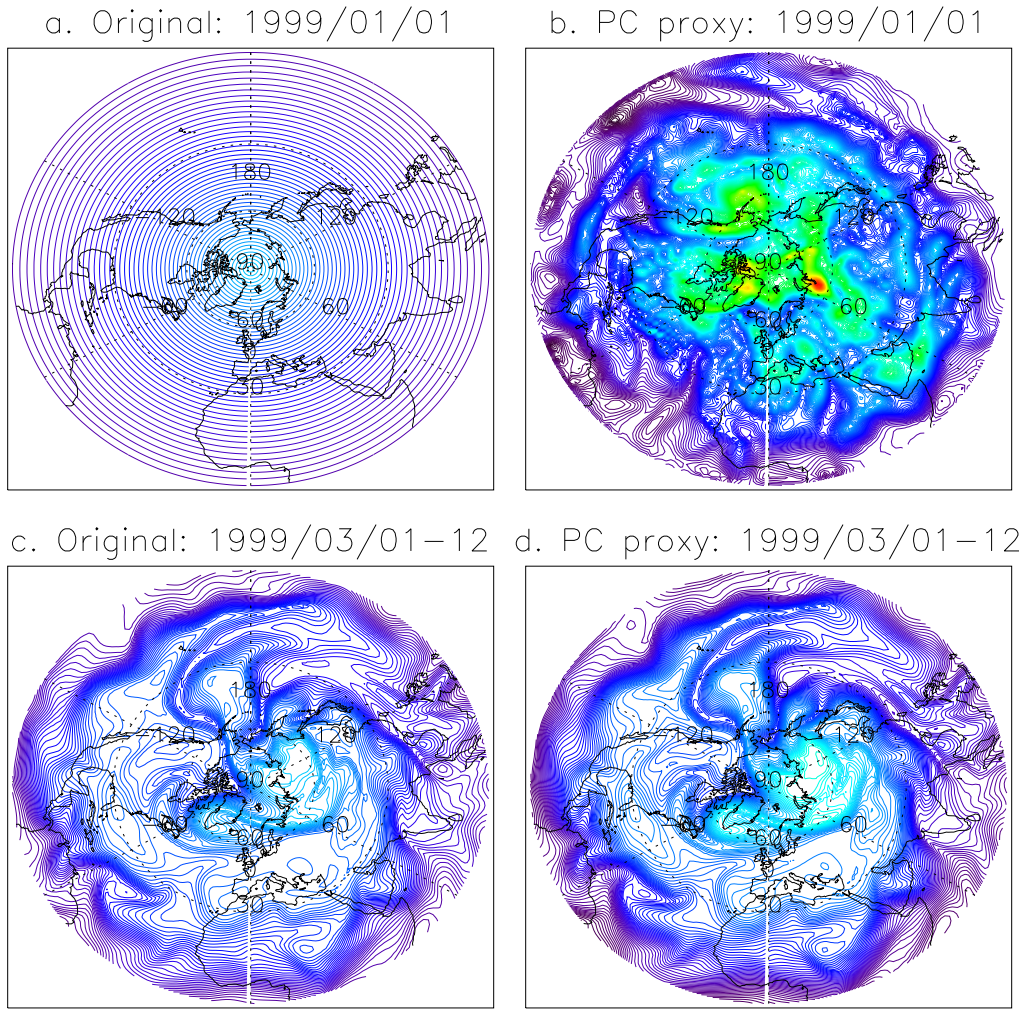


Figure 4: Comparison of simulated tracer fields with the reconstructed version. a. and b. compare the initial field of the simulated versus the reconstructed, respectively, while c. and d. compare the fields at the lead time, 60 days later.



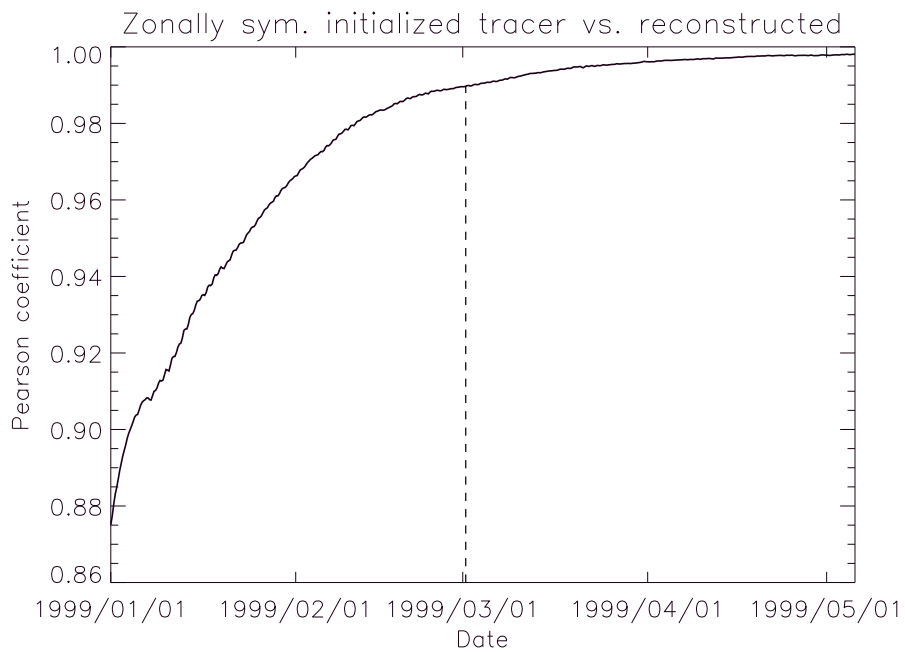


Figure 5: Correlation over time of a zonally-symmetric-initialized, passive tracer with one reconstructed using PC proxy using a lead time of 60 days, marked by the vertical, dashed line.

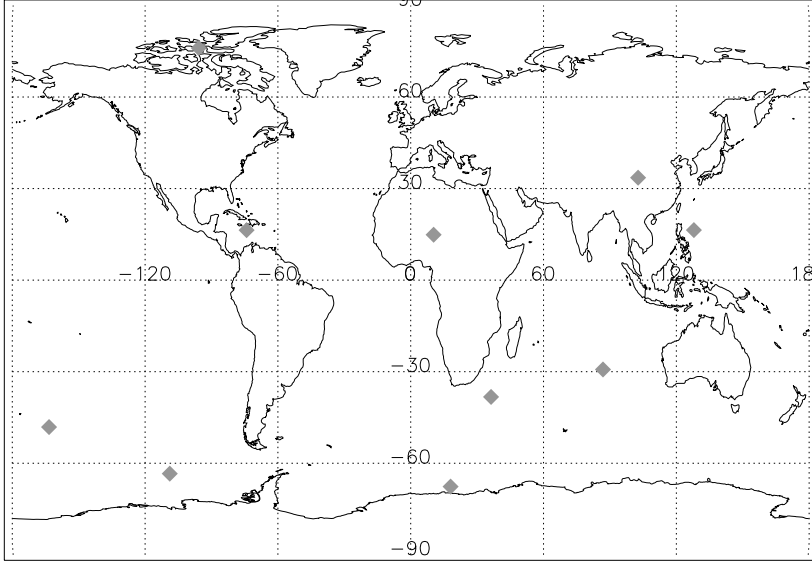


Figure 6: Locations of the ten (10) simulated sparse measurements used for the test retrieval.

vected before performing the SVD. Measurements are selected within the measurement window which is centered at the end of the lead time.

Figure 4 and 5 shows the results of a test retrieval for a zonally-symmetric-initialized tracer using a lead time of 60 days and five singular vectors. The Lyapunov spectrum can help us select the number of singular vectors as it shows how many remain significant at a given lead time—see Figure 3. Ten sparse measurements were randomly selected in space and time within a measurement window of one day—these are plotted in Figure 6. The Pearson correlation for the initial field (Figures 4a. and b.) is 0.875, while the correlation at the lead time (Figures 4c. and d.) is 0.99

## 6 Ozone reconstruction

The purpose here is not to perform a rigorous validation, but rather to demonstrate *proof-of-concept*. To do this we perform a cross-validation exercise on Polar Ozone and Aerosol Measurement (POAM) III satellite retrievals

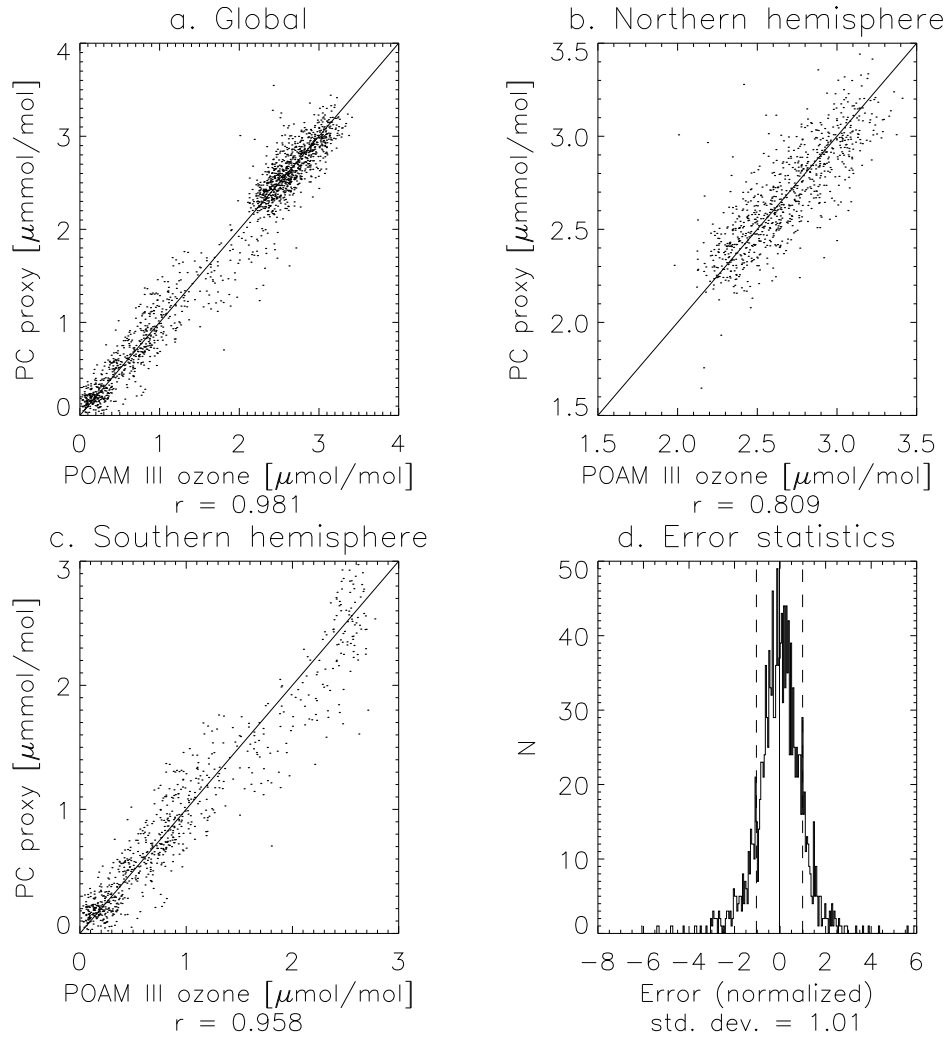


Figure 7: a. Scatter plot of PC proxy cross-validation results with POAM III ozone data on the 500 K isentrop for November and December 1998, 60 day lead time and 2 day measurement window. b. and c. show comparison results restricted to Northern and Southern hemisphere respectively. c. Histogram of errors normalized by original error estimates from the POAM inversion. The solid vertical lines shows the average, while the dashed lines show the standard deviation.

(Lucke et al., 1999) in which the data is divided into two parts: a *training* data set and a *test* data set. The two are divided approximately evenly: each measurement is selected at random to go into one or the other set. The analysis is done once again at the 500 K isentropic level; a lead time of 60 days and a measurement window of 2 days is used.

Validation results are shown in Figure 7. Unlike in Randall et al. (2002), the reconstruction is done over the entire globe. Since ozone concentrations are generally lower in the Southern hemisphere, this will produce an artificially high skill score, thus we also include comparisons limited to each of the two hemispheres. Figure 7d. shows the error statistics, normalized by the original error from the POAM inversion (Lumpe et al., 2002). Note that the standard deviation for this error is almost exactly one (1), meaning that the error for the reconstructed ozone is about the same as the original measurement error.

Finally, we compare the ozone fields reconstructed from the POAM data with ozone sonde measurements from the World Ozone Data Centre (WODC) (Hare et al., 2000). Validation results are shown in Figure 8. Once again, the comparison is done for both Northern and Southern hemispheres exclusively, using the globally reconstructed ozone, and error statistics are shown in the final figure, 8d. Root-mean-square error for the ozone sondes is  $0.45 \mu\text{mol/mol}$  (volume-mixing-ratio (vmr) in parts-per-million (ppm): ppmv) while for the cross-validation (statistics are graphed with the dotted line) it is  $0.20 \mu\text{mol/mol}$ .

A sample reconstructed ozone field is shown in Figure 9, Note that for the sample field, values towards the equator and the lower latitudes are suspect, discussed in more detail in Section 7, below. The launch stations are plotted on the field and, like the POAM measurements, are mostly restricted to the higher and mid-latitudes.

## 7 Discussion and conclusions

Further work needs to be done to determine the optimal number of PCs to use in an analysis as well as the optimal lead times. Preliminary work shows that beyond a lead time of about 60 days, skill scores differ little. Presumably, reconstruction of shorter-(longer-)lived tracers would work better with shorter (longer) lead times. Naturally, a longer lead time means longer compute times. The number of PCs required will be related in part to the lead

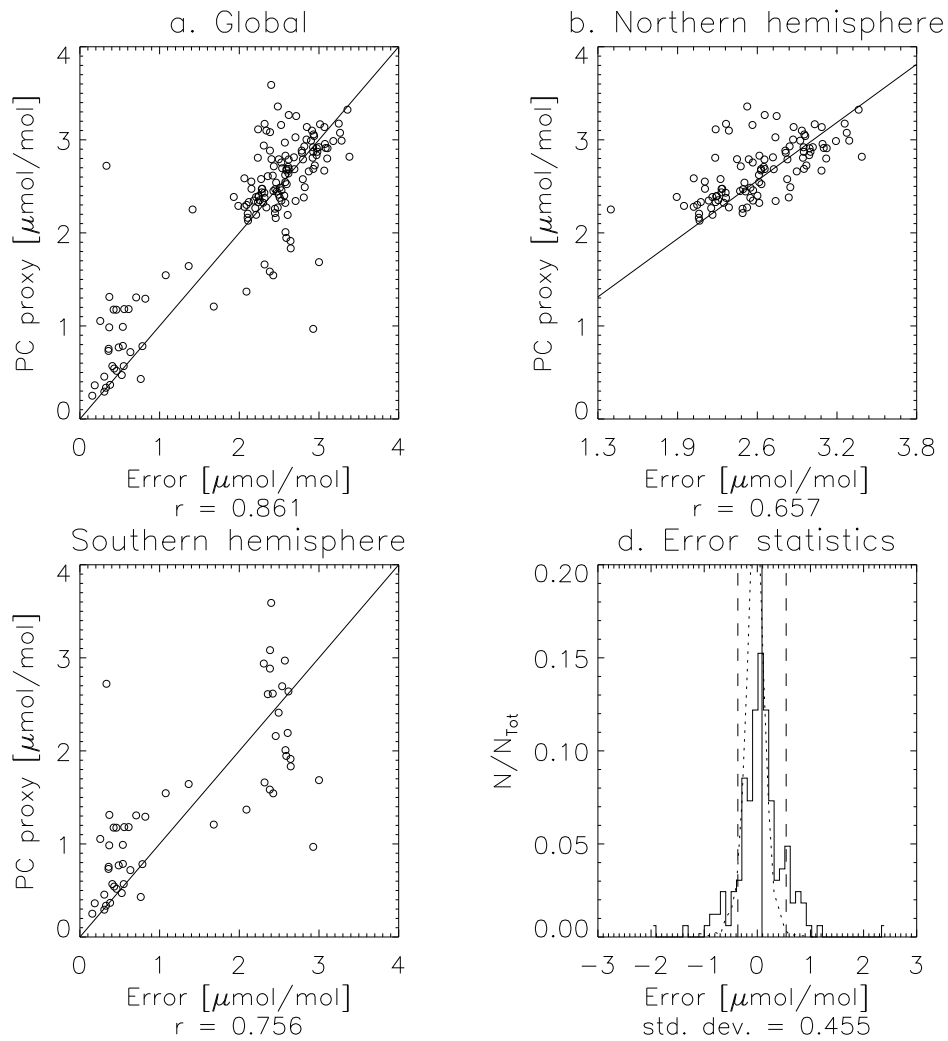


Figure 8: Ozone reconstructed from POAM versus ozone sonde data. Figures b. and c. restrict the comparison to the Northern and Southern hemispheres respectively. Figure d. shows error statistics (histogram bars). Solid vertical line is the average, while the dashed lines show the standard deviation. Error statistics for the cross-validation are shown for comparison (dotted line).

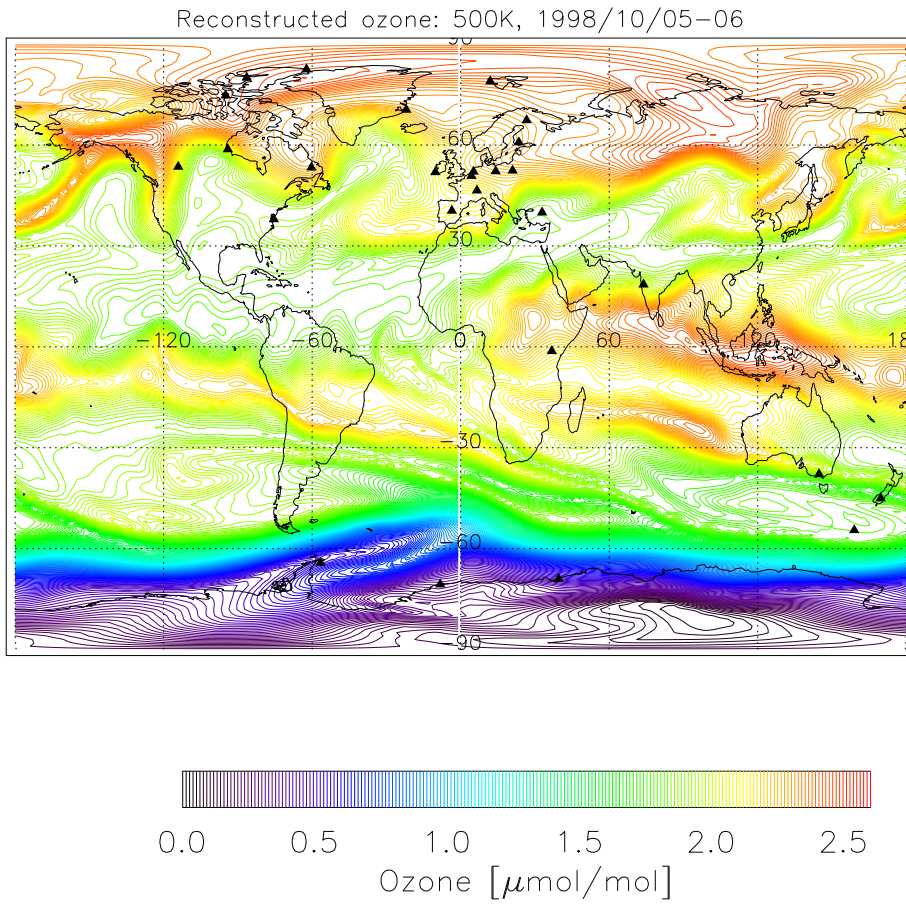


Figure 9: Sample ozone field reconstructed using the PC proxy technique from POAM III data at the 500 K isentrop. Triangles show the locations of the ozone sonde launch stations used in the validation exercise.

time, as discussed in Section 5, with shorter lead times requiring more PCs. Obviously, a larger number of measurements will support the use of more PCs.

Another problem in some of the reconstructed fields is that the solution tended to blow up towards the equator, showing ringing, negative concentrations, and other artifacts. Including a constant term in the fitting procedure did little to alleviate the problem. A better solution would be to use some form of regularization to constrain the solution, as in optimal estimation (Rodgers, 2000), or better still, include more measurements in the analysis. Most of the ozone sondes were also launched in the higher latitudes, so this did not significantly affect the comparison results.

Nonetheless, principal-component (PC) proxy tracer analysis is shown to be a powerful, dynamical interpolation method capable of reconstructing a passive tracer using as few as ten (10) sparse measurements. Ozone reconstructed from the Polar Ozone and Aerosol (POAM) III instrument showed reasonable agreement with ozone sondes, despite using, on average, 52 measurements per field and these limited to a narrow latitude bands in either hemisphere.

The method has the advantage over more tradition proxy tracer analysis in that it provides more degrees of freedom from the higher principal components thus can account for more recent changes in the tracer.

The ozone reconstruction for the cross-validation exercise was so good, in fact, that the errors were of the same order as the original POAM retrievals, suggesting that these error estimates are too high to begin with.

Software for this project can be found at: <http://ctrjaj.sf.net>.

## Acknowledgements

Thanks to the National Center for Environmental Prediction (NCEP) for re-analysis data and to my former colleagues at the Naval Research Laboratory for POAM data. Thanks also to the World Ozone Data Centre (WODC) for radiosonde ozone data.

The author would also like to thank John Lin of the University of Waterloo for partially supporting this work and the Institute of Environmental Physics, University of Bremen for the use of their computers.

## References

- Allen, D. R. and Nakamura, N. (2003). Tracer Equivalent Latitude: A Diagnostic Tool for Isentropic Transport Studies. *Journal of the Atmospheric Sciences*, 60:287–303.
- Galassi, M., Davies, J., Theiler, J., B. Gough, B., Jungman, G., Booth, M., and Ross, F. (2007). *GNU Scientific Library: Reference Manual*. Available online at: <http://www.gnu.org/software/gsl>.
- Golub, G. H. and van Loan, C. F. (1996). *Matrix Computations*. Johns Hopkins University Press.
- Hare, E. W., Carty, E. J., and Wardle, D. I. (2000). Guide to the WMO/GAW world ozone data centre. Technical report, Meteorological Service of Canada, Environment Canada.
- Kalnay, E., Kanamitsu, M., Kistler, R., Collins, W., Deaven, D., Gandin, L., Iredell, M., Saha, S., White, G., Woollen, J., Zhu, Y., Chelliah, M., Ebisuzaki, W., Higgins, W., Janowiak, J., Mo, K., Ropelewski, C., Wang, J., Leetmaa, A., Reynolds, R., Jenne, R., and Joseph, D. (1996). The NCEP/NCAR 40-year reanalysis project. *Bull. Amer. Meteor. Soc.*, 77:437–470.
- Lehoucq, R. B. and Scott, J. A. (1996). An Evaluation of Software for Computing Eigenvalues of Sparse Nonsymmetric Matrices. Technical Report MCS-P547-1195, Argonne National Laboratory.
- Lucke, R. L., Korwan, D. R., Bevilacqua, R. M., Hornstein, J. S., Shettle, E. P., Chen, D. T., Daehler, M., Lumpe, J. D., Fromm, M. D., Debresian, D., Neff, B., Squire, M., Knig-Langlo, G., and J. Davies, J. (1999). The Polar Ozone and Aerosol Measurement(POAM) III instrument and early validation results. *Journal of Geophysical Research*, 104(D15):18785–18799.
- Lumpe, J. D., Bevilacqua, R. M., Hoppel, K. W., and Randall, C. E. (2002). POAM III retrieval algorithm and error analysis. *Journal of Geophysical Research*, 107(D21):ACH5.1–ACH5.32.
- Mills, P. (2009). Isoline retrieval: An optimal method for validation of advected contours. *Computers & Geosciences*, 35(20):2020–2031.



- Ott, E. (1993). *Chaos in Dynamical Systems*. Cambridge University Press.
- Press, W. H., Teukolsky, S. A., Vetterling, W. T., and Flannery, B. P. (1992). *Numerical Recipes in C*. Cambridge University Press, 2nd edition.
- Randall, C. E., Lumpe, J. D., Bevilacqua, R. M., Hoppel, K. W., Fromm, M. D., Salawitch, R. J., Swartz, W. H., Lloyd, S. A., Kyro, E., von der Gathen, P., Claude, H., Davies, J., DeBacker, H., Dier, H., Molyneux, M. J., and Sanchoi, J. (2002). Reconstruction of three-dimensional ozone fields using POAM III during SOLVE. *Journal of Geophysical Research*, 107(D20):8299–8312.
- Rodgers, C. D. (2000). *Inverse Methods for Atmospheric Sounding: Theory and Practice*. World Scientific.
- Tang, Y. R., Kleeman, R., and Miller, S. (2006). ENSO predictability of a Fully Coupled GCM Model Using Singular Vector Analysis. *Journal of Climate*, 19(14):3361–3377.